

Uncertainty assessment for reconstructions based on deformable geometry

K.M. Hanson, G.S. Cunningham, and R.J. McKee*
Los Alamos National Laboratory, MS P940
Los Alamos, New Mexico 87545 USA

ABSTRACT

Deformable geometric models can be used in the context of Bayesian analysis to solve ill-posed tomographic reconstruction problems. The uncertainties associated with a Bayesian analysis may be assessed by generating a set of random samples from the posterior, which may be accomplished using a Markov-Chain Monte-Carlo (MCMC) technique. We demonstrate the combination of these techniques for a reconstruction of a two-dimensional object from two orthogonal noisy projections. The reconstructed object is modeled in terms of a deformable geometrically-defined boundary with a uniform interior density yielding a nonlinear reconstruction problem. We show how an MCMC sequence can be used to estimate uncertainties in the location of the edge of the reconstructed object.

Keywords: Bayesian estimation, deformable geometric models, tomographic reconstruction, uncertainty estimation, Markov Chain Monte Carlo

1. INTRODUCTION

Deformable geometric models are increasingly being used to analyze medical images. Their use is motivated by the desire to represent natural characteristics of objects in the real world. Furthermore, deformable models can provide the regularization needed to solve ill-posed problems.^{1,2} The smoothness of deformable models is typically controlled by means of a deformation energy function.³ In the context of Bayesian analysis, the probability of the corresponding geometric configuration is taken to be proportional to the negative exponential of this energy function.⁴

The main theme of this paper concerns the assessment of uncertainties in estimated models, a capability greatly assisted by the use of Bayesian analysis. The general method we employ here to estimate uncertainty in a reconstructed object is to generate a sequence of random samples of the posterior probability distribution using the Markov Chain Monte Carlo (MCMC) technique. By fully mimicking the posterior, this sequence of samples can be used to assess the posterior in various ways. As an example of the usefulness of this technique, we consider a problem of reconstructing an object from projections in two directions under the assumption of a known, uniform interior density. In the analysis, the boundary of the reconstructed objects are subject to a prior that promotes smoothness. We show how the MCMC samples from the posterior can be used to estimate uncertainties in the location of the boundary of the reconstructed object.

We deliberately chose our example of tomographic reconstruction from two views because this extremely difficult problem can not be solved with conventional reconstruction algorithms, as shown in Ref. 5, for example. Our ability to obtain an excellent reconstruction emphasizes the advantage of using deformable models in tomography when objects have a relatively simple shape and possess uniform density. MCMC provides the means to verify the reliability of our reconstruction. Conventional approaches to uncertainty estimation are not adequate to treat this problem because of the nonlinear relation between the data and the model parameters and, hence, the potential nonGaussian nature of the posterior distribution.

Supported by the United States Department of Energy under contract W-7405-ENG-36.
Email: kmh@lanl.gov, cunning@lanl.gov, mckee@lanl.gov; WWW: <http://home.lanl.gov/kmh/>

2. BAYESIAN ANALYSIS

Bayesian analysis provides the ultimate means of the analysis of uncertainties in the interpretation of data with respect to models. Every aspect of modeling is assigned a probability that indicates our degree of certainty about it. At the lowest level of analysis, the estimation of the values of parameters for a specified model, a probability density function (PDF) is associated with each continuous parameter. Loosely speaking, the range of a probability distribution indicates the possible range of its associated parameter. The benefit of Bayesian analysis over traditional methods of uncertainty analysis is that it permits the use of arbitrary probability distributions, not just Gaussian distributions, and of arbitrary measures of uncertainty, not just rms deviation (or variance). Bayesian analysis reveals the use of prior knowledge and assumptions, which other kinds of analysis incorporate, but do not always make explicit. Furthermore, it extends analysis to higher levels of interpretation, e.g., the choice of the strength of the priors used, the rejection of any particular model, and the selection of appropriate models.⁶ For detailed descriptions of Bayesian analysis the reader is referred to the several excellent recent books.^{7,8}

Before conducting an experiment, one starts with some knowledge about the physical object being studied. In addition one often has in mind a model for the object, with associated parameters \mathbf{x} , that will be used to analyze the experimental results. In Bayesian analysis, the uncertainties in what is known beforehand are expressed in terms of a PDF on the parameters, $p(\mathbf{x})$, called the prior. This prior knowledge can come from previous measurements, specific information regarding the object itself, or simply general knowledge about the parameters, e.g., that they are nonnegative. With the experimental data in hand, the prior is modified to yield the posterior, which is the PDF $p(\mathbf{x}|\mathbf{d})$ of the parameters given the observed data \mathbf{d} , using Bayes law

$$p(\mathbf{x}|\mathbf{d}) \propto p(\mathbf{d}|\mathbf{x}) p(\mathbf{x}) . \quad (1)$$

The probability $p(\mathbf{d}|\mathbf{x})$, called the likelihood, comes from a comparison of the actual data to the data predicted on the basis of the model of the object. The predicted data are generated using a model for how the measurements are related to the object, which we call the measurement model. Under the assumption that the data are degraded by uncorrelated and additive Gaussian noise, the likelihood should be proportional to the exponential of $-\frac{1}{2}\chi^2$. As usual, χ^2 is the sum of the squared differences between the actual and the predicted measurements divided by the variance in the measurement noise. Often the model that maximizes the posterior, referred to as the maximum *a posteriori* (MAP) estimate is found, although other estimators can be argued to be more appropriate in some circumstances. While an estimate of the best model is the objective of many analyses, it is only the beginning for the true Bayesian.

Bayesian analysis is open ended. If the preconceived object model fails to account for the data, the model may need to be extended, or even replaced. Model checking is an important aspect of any data analysis. Of course, the data may not be accurate enough to reject a particular model, in which case the model can be considered valid until more discriminating data are available. Bayesian analysis follows the scientific method; a proven model is used until reliable data indicate that it needs to be altered or rejected. Bayes law can be used to choose between models.⁶

2.1. Deformable models

We wish to focus on the geometry or shape of objects. To this end, we use a deformable model to represent the boundary of the objects to be reconstructed. Their interior density can often be taken to be uniform. The boundary is approximated in discrete terms as a finely-divided polygon. This kind of model actually imposes desirable constraints on the object's boundary: that it is connected and continuous and that it has a sharply-defined edge.

Smoothness of the boundary is achieved by placing a prior on the curvature of the boundary. The minus-log-prior is taken to be proportional to $\int \kappa^2(s) ds$, where $\kappa(s)$ is the curvature of the curve as a function of the arclength s . This form has a physical analog in the formula that describes the potential energy created by bending a stiff rod. Since the integral has the dimensions of reciprocal length, it depends on the scale of the curve. To achieve a prior that is related to the shape of the curve, not its size, the integral should be multiplied by the total arclength of the boundary, forming a dimensionless quantity. From the Bayesian point of view, the prior is interpreted probabilistically. A specific probability is assigned to every closed boundary,

which ranks boundary shapes according to their plausibility. This probability expresses the uncertainty about the possible shapes of the object that we have before we take data, as visually demonstrated in Ref. 9.

For our discrete polygon model, we replace the integral by a sum of contributions associated with each vertex in combination with half of each neighboring edge of the polygon. To approximate $\int ds \int \kappa^2(s) ds$ for the continuous curve, we use for the minus-log-prior the expression

$$\alpha \frac{1}{2\pi} \left[\sum_j L_j^+ \right] \left[\sum_j 2w_j \frac{\tan^2(\theta_j/2)}{L_j^- L_j^+} (L_j^- + L_j^+) \right], \quad (2)$$

where the sums are over the vertices of the polygon, $\pi - \theta_j$ is the internal angle at the j th vertex, L_j^- and L_j^+ are the lengths of the previous and next edge of the polygon, and w_j is the weight for the j th vertex. The factor of $(2\pi)^{-1}$ normalizes the expression so it equals $2\pi\alpha$ for a circle. The parameter α , called a hyperparameter rather than a parameter because it controls a general aspect of the model, determines the strength of the prior relative to the likelihood. See Ref. 10 for details.

In addition to the smoothness constraint, we find it necessary to control the lengths of the sides of the polygon to keep them nearly equal. This control is accomplished by adding to the above minus-log-prior the expression $\frac{\beta}{n} \sum_j [(L_j^+ - \bar{L})/\bar{L}]^2$, where $\bar{L} = \frac{1}{n} \sum_j L_j^+$ is the average length of the n sides of the polygon. The choice for the hyperparameter β should be relatively unimportant because this prior only provides control of the polygon representation. The value $\beta = 100$ seems to work well in the present circumstance.

We believe there is a significant benefit in using the finely-divided polygon representation instead of often-used alternatives, such as B-spline or Bezier patches. A polygon can approximate a curve to any desired accuracy by subdividing the sides finely enough. However, by itself, a polygon has no constraint on its shape. In our approach, a quasi-smooth curve is achieved by introducing a prior. Here we use for the minus-log-prior the integral of the square of the curvature. Constraints other than on the curvature may be used, such as requiring that the curve not intersect itself. The advantage of this overall approach is that alternative forms for the prior can be assessed for any particular imaging situation.

An alternative to this approach is to restrict the flexibility of the model through the choice of a more restrictive representation. For example, one could choose polynomial patches, where each patch has a limited number of degrees of freedom determined by the order of polynomial chosen. Then the flexibility of the curve is controlled by the order of polynomial and/or number of patches. One has only limited and discrete control in this approach.

Our approach has the major advantage of allowing continuously tunable control over the flexibility of the boundary. The strength of the prior (α in the preceding discussion) regulates the effective number of degrees of freedom that the curve has, much in the same way as the number of patches in a Bezier representation. Furthermore, one may vary the weight w_j in Eq. (2) to encourage the curve to be smooth in some regions and very flexible in others. Indeed, when the data or prior knowledge demand it, one can induce a kink in the curve by setting the weight to zero.¹⁰

The present study is carried out using the Bayes Inference Engine (BIE). We developed the BIE to allow one to easily construct complex models for both the objects under study and the measurement process.^{5,11–13} The MCMC technique is a perfect match to the computational approach to Bayesian inference adopted in the BIE.¹⁴

3. MARKOV CHAIN MONTE CARLO

The Markov Chain Monte Carlo (MCMC) technique provides a means to sample an arbitrary probability density function (PDF). A desirable attribute of MCMC is that there are generally no restrictions on the types of PDFs. In its basic form, MCMC only requires that one be able to calculate the PDF.

A Markov chain is a sequence of states in which the probability of each state depends only on the previous state. In MCMC the objective is to generate a sequence of parameter sets that mimic a specified PDF, let's call it $q(\mathbf{x})$, where \mathbf{x} is a vector of parameters in the relevant parameter space. More precisely,

it is desired that the MCMC sequence be in statistical equilibrium with $q(\mathbf{x})$, which is achieved when the MCMC sequence satisfies the condition of detailed balance:

$$q(\mathbf{x})T(\mathbf{x} \rightarrow \mathbf{x}') = q(\mathbf{x}')T(\mathbf{x}' \rightarrow \mathbf{x}) , \quad (3)$$

where $T(\mathbf{x} \rightarrow \mathbf{x}')$ is the MCMC transition probability for stepping from \mathbf{x} to \mathbf{x}' . This equation essentially requires that in a very long sequence the number of steps from \mathbf{x} to \mathbf{x}' is identical to the number from \mathbf{x}' to \mathbf{x} . For more information about MCMC, see the recent paper by Besag et al.¹⁵ or the excellent book edited by Gilks et al.¹⁶

The MCMC technique¹⁵ makes it feasible to perform some of the difficult technical calculations required by probability theory (normalization of PDFs, marginalization, computation of expectation integrals, model selection) in a computer. MCMC is one of the important tools that will allow Bayesian analysis to be conducted on the complex models demanded in many application areas.

3.1. Metropolis algorithm

One of the simplest algorithms used in MCMC calculations is due to Metropolis et al.¹⁷ This algorithm ensures detailed balance (3) for each step in the sequence. One starts at an arbitrary point in the vector space to be sampled, \mathbf{x}_0 . The general recursion at any point in the sequence \mathbf{x}_k is as follows:

- (1) Pick a new trial sample $\mathbf{x}^* = \mathbf{x}_k + \Delta\mathbf{x}$,
where $\Delta\mathbf{x}$ is randomly chosen from a symmetric probability distribution
- (2) Calculate the ratio $r = q(\mathbf{x}^*)/q(\mathbf{x}_k)$
- (3) Accept the trial sample, that is, set $\mathbf{x}_{k+1} = \mathbf{x}^*$,
if $r \geq 1$,
or with probability r , if $r < 1$,
otherwise start over at step (1).

For being so simple, it is remarkable that this algorithm works quite well!

We will demonstrate the power of MCMC to assess Bayesian model uncertainties by sampling the posterior in an example involving tomographic reconstruction. We will finish up by discussing some of its weaknesses in the last section.

3.2. Simulation of repeated experiments

An alternative approach that is often used to characterize and test a reconstruction algorithm is based on the simulation of repeated experiments. The algorithm is used to obtain reconstructions from several sets of simulated measurements, each of which contain new realizations of the noise. This approach provides insight into the propagation of noise in a reconstruction algorithm. However, it does not fully explore the uncertainty of the reconstruction for underdetermined problems. Basically, this approach characterizes the estimator, averaged over noise realizations.

Consider a reconstruction problem in which the measurements are linearly related to the parameters to be estimated; the vector of measurements can be written as the product of a measurement matrix times the parameter vector. In ill-determined reconstruction problems, the measurement matrix possesses a null space, which means that there exist combinations of parameters that do not affect the measurements. Parameter vectors that lie wholly in the null space of the measurement matrix are sometimes called ghosts. These parameter sets are not determined by the data. The prior information should help fill in the null-space components of the parameter space with something meaningful.^{18,19}

It is easy to show that the above simulation approach does not sample the uncertainties in the null space. However, the MCMC approach can do so because it randomly samples the parameter space. As such, it can also incorporate uncertainties that arise from the priors. The use of multiple hypothetical data sets is a foreign concept in the Bayesian assignment of uncertainties. In practice, one has only one data set with which to work and that is the *modus operandi* of Bayesian analysis. In fact there are likelihood functions that depend on the actual data that one has, for example, counting data described by the Poisson distribution²⁰ or samples from the Cauchy distribution.²¹ The uncertainties in analyzing such data sets can vary from one data set to the next. In these situations, it makes little sense to average over multiple data sets except to



Figure 1. The original object used in the example.

characterize the average uncertainty one might expect for an anticipated experiment. On the other hand, it is legitimate to use multiple data sets and multiple objects to characterize the long-term performance of Bayesian algorithms.²²

4. EXAMPLE

4.1. Problem statement

We demonstrate the versatility of the MCMC technique with an example of tomographic reconstruction from just two views. This problem is known generally to be an extraordinarily difficult inverse problem. Its solution is made feasible by employing the prior information that the object being reconstructed has uniform density and consists of a fairly simple shape with smooth boundaries. Figure 1 displays the object concocted for this example. It is fashioned to be representative of the cross section of an occluded artery. The calculations here are based on images with a full width of 128×128 pixels, arbitrarily set to a size of $4 \text{ mm} \times 4 \text{ mm}$. For better visualization, all the images shown here display just the central $2.5 \text{ mm} \times 2.5 \text{ mm}$ region. To give the scale of the images, the width and height of the object are roughly 64 pixels, or about 2 mm.

Two orthogonal views of the object are generated under the assumption of no measurement-system blur. Each projection consists of 128 samples over a distance of 4 mm. Gaussian noise is added to these projections with an rms deviation of 5% of the peak projection amplitude.

4.2. MAP reconstruction

For reconstruction the object is modeled in terms of a finely-divided polygon filled with a uniform density, which we assume is known beforehand. The polygon has 50 sides to approximate a continuous curve. The parameters in the model consist of the x and y values of the 50 vertices. The $-\log(\text{posterior})$ for this problem is the sum of $-\log(\text{likelihood}) = \frac{1}{2}\chi^2$ and the $-\log(\text{prior})$ contributions given in Sect. 2.1. However, the strength of the prior, i.e. α in Eq. (2), must be specified. Ideally, the hyperparameter α that is consistent with the data would be calculated utilizing the next higher level of Bayesian inference.⁶ As we are not yet equipped to do that in the BIE, we tried several values for α and selected what seemed to be an appropriate value, $\alpha = 1.0$. See below for further justification.

The MAP reconstruction is obtained by using the BIE to find the minimum in $\varphi = -\log(\text{posterior})$ with respect to the 100 variables specifying the polygon model. The BIE accomplishes this in an efficient manner

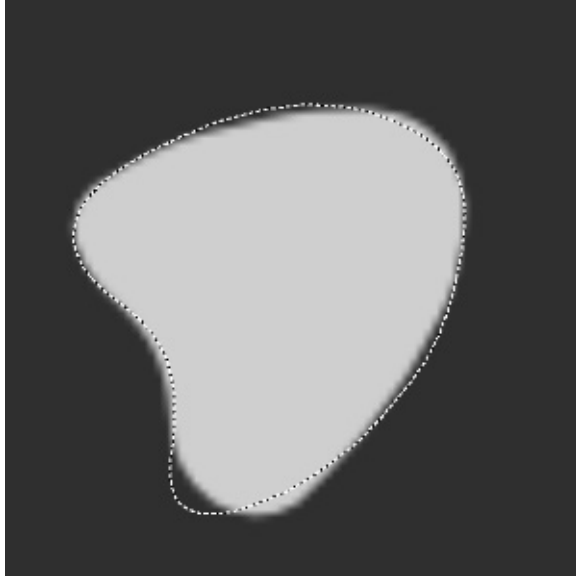


Figure 2. The MAP reconstruction from two orthogonal noisy projections, shown as a grayscale image with the boundary of the original object superimposed.

through the use of the Adjoint Differentiation In Code Technique (ADICT)¹⁴ to calculate the gradient of φ with respect to the variables. The initial object is taken to be a circle of diameter 1.6 mm = 51 pixels, for which $\frac{1}{2}\chi^2 = 396.15$ and $-\log(\text{prior}) = 6.28$. At the minimum in φ , these values are $\frac{1}{2}\chi^2 = 119.16$, and $-\log(\text{prior}) = 18.24$. The resulting reconstructed object compares reasonably well with the original, as shown in Fig. 2. The maximum discrepancy in the position of the two boundaries is about 3.3 pixels, which occurs in the lower lobe. Over the vast majority of the perimeter, the reconstructed boundary lies less than one pixel away from the original.

The reconstruction shown in Fig. 2 is vastly superior to one that would be obtained using conventional reconstruction algorithms.⁵ We will now assess the reliability of this reconstruction by using MCMC to assess its uncertainty.

4.3. MCMC results

The MCMC algorithm described above was used to generate samples from the posterior of this reconstruction problem. In our present example, for each MCMC trial step, the increments in the x and y position of each of the vertices are independently chosen from a Gaussian distribution with an rms step size of 0.06 pixels. Since we are drawing samples from the space of x and y and the priors outlined in Sect. 2.1 are stated in the θ, L space, we would need to transform from $p(\theta, L)$ to $p(x, y)$ using the Jacobian of the transform to properly evaluate the priors for the MCMC algorithm. This Jacobian would alter the approximately quadratic form of Eq. (2) by adding terms that are approximately constant for small θ s. We believe these terms amount to relatively minor adjustments in the values of the priors and so ignore them.

In all, 150,000 trial steps are calculated and 42049 steps were accepted, for an acceptance rate of about 28%. This calculation takes about 16 hours on a DECstation 250 with a DEC 266-MHz-Alpha processor. Three widely-separated samples from the full MCMC sequence are shown in Fig. 3. While it is not possible to deduce any quantitative behavior from these three samples, they provide some indication of the amount of variation in the shapes that occupy the posterior. The amount of waviness observed in the boundary is moderate, as can be observed in Fig. 3. The superfluous waviness compared to the original object is evidence that $\alpha = 1$ is a safe choice, i.e. it is weak enough that it does not exert an undue influence on the shape of the MAP solution.

During the generation of the MCMC sequence, the configuration of the boundary is saved at every fiftieth step in the sequence. After the full sequence is generated, the saved configurations can be played

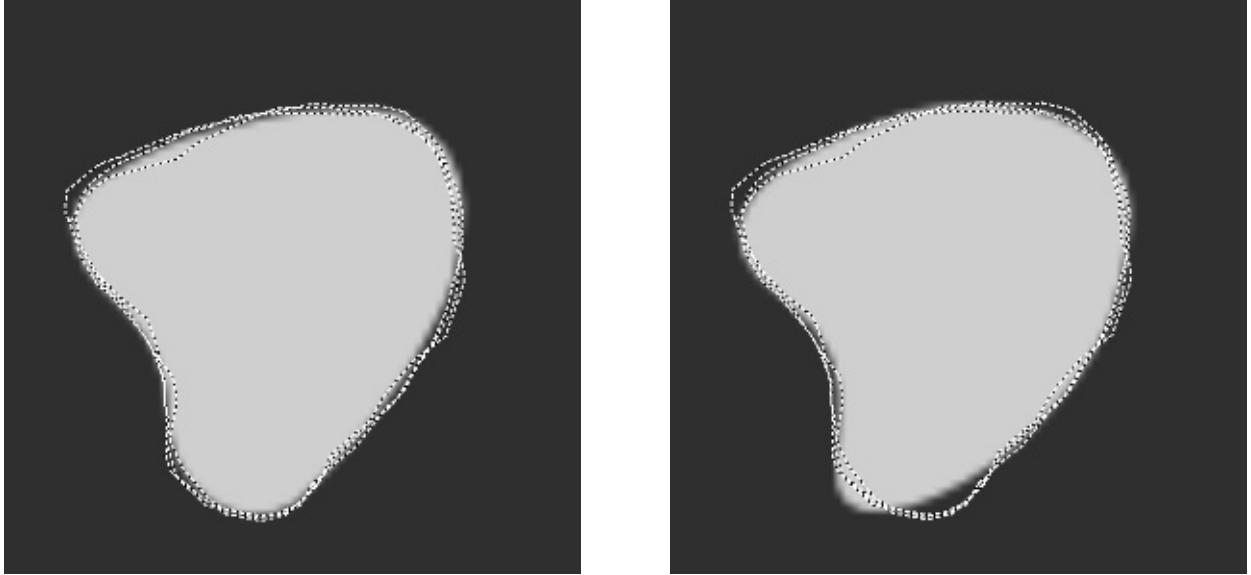


Figure 3. Three representative samples from the posterior shown as curves on top of the grayscale images of (a) the MAP reconstruction and (b) the original object.

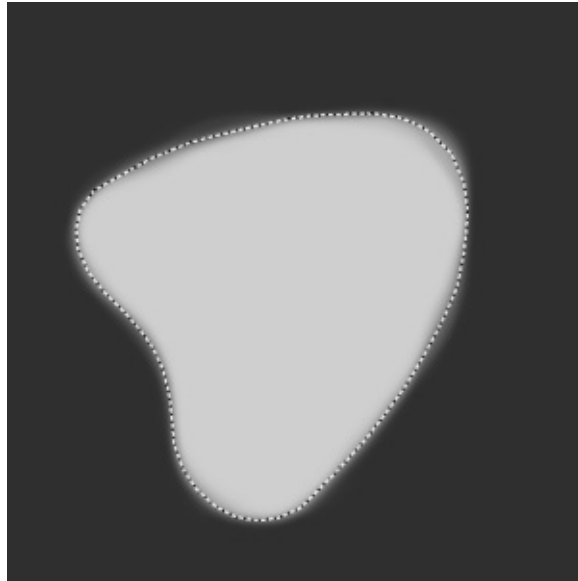


Figure 4. The average of the grayscale images for full MCMC sequence of samples from the posterior with the contour for the MAP reconstruction shown as a dotted line.

back as a video loop. Visual observation of the abridged sequence indicates that there is a strong correlation in the configurations over a few frames, that is, over more than a hundred steps in the sequence. This correlation might be expected because of the very small step that each vertex can take in each iteration of the Metropolis algorithm. We observe from the video loop that it takes several hundred steps in the sequence for the boundary to move from plus to minus one standard deviation about the mean position, a distance of a few pixels. Roughly speaking, one might expect that it would take on the order of $[2/(0.06\sqrt{2})]^2 \approx 500$ random steps of rms radial distance $0.06\sqrt{2}$ pixels to move a total distance of two pixels.

A quantitative estimate of the characteristics of the posterior is obtained by averaging over the MCMC

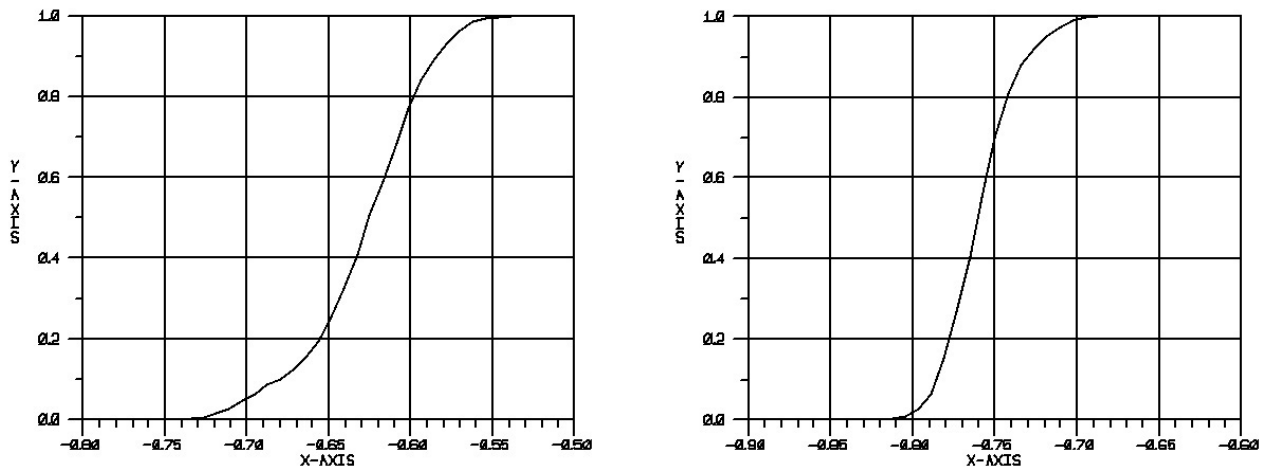


Figure 5. Vertical edge profiles of the MCMC average image at two positions along the top edge of the object, (b) at the apex of the reconstruction and (a) midway between that point and the left edge. The horizontal grid spacing of the plot, 0.05 mm, corresponds to 1.6 pixel widths.

sequence. Such an average of the grayscale image of the object is shown in Fig. 4, which is calculated as an overlap of the boundary interior with the pixels of a 512×512 image for increased resolution. Of course, it does not make sense to average the positions of the vertices, because there is nothing to keep the polygon from slipping around the boundary of the object, which has no bearing on the actual object shape. The average MCMC image in Fig. 4 represents the posterior mean image. The amount of blur in the edge of the object, e.g., as shown in Fig. 5, indicates the variability in the position of that edge allowed by the posterior, i.e. the uncertainty in edge location. From the measured distance between the 10% and 90% points of the blurred edge of this posterior average, we deduce that the rms uncertainty in edge location varies from about 0.5 pixels to about 1.0 pixels at various positions around the periphery. The smallest rms deviations occur at the limiting edges on the top, bottom, and right sides of the object. The smaller uncertainty at these positions appears to be a consequence of the fact that they are effectively located by the tangential rays of the two projections. The horizontal position of the left edge is not quite as well determined. Of course, it is possible to measure correlations between the uncertainties at different positions.

Figure 4 also shows that the MAP reconstruction (the model that maximizes the posterior) appears to be consistent with the contour at half the amplitude of the posterior mean image. This result suggests that the posterior probability distribution is symmetric about its maximum. From the shape of the edge profile of the posterior average, for example shown in Fig. 5, we tentatively conclude that the posterior may approximately be a multivariate Gaussian distribution, despite the nonlinear relation between the vertex parameters and the measurements.

One of the largest rms deviations is found to be along the top arc, just left of the middle, as shown in Fig. 5a. This large uncertainty is caused by the ability of the top boundary of the object to easily move left and right and still match the data fairly well. This movement is feasible because it can be matched by small distortions in other parts of the boundary, an effect that can be observed in the video loop.

An interesting and important feature of the MCMC technique is that any feature that one wishes to characterize, e.g., the average edge position and its uncertainty in the above example, is not conditional on the other parameters in the model. In the terms of probability theory, MCMC provides marginalized results, which means that the dependence on the uncertainties in “nuisance variables” is integrated out. In the context of the above example, the uncertainty in the edge position deduced for any particular location of the boundary is independent of the uncertainties in edge positions for the rest of the boundary.

The MCMC average image, Fig. 4, may be interpreted as a probability image; the value of each pixel is the posterior probability that the pixel lies inside the boundary of the object. The pixels that have a value

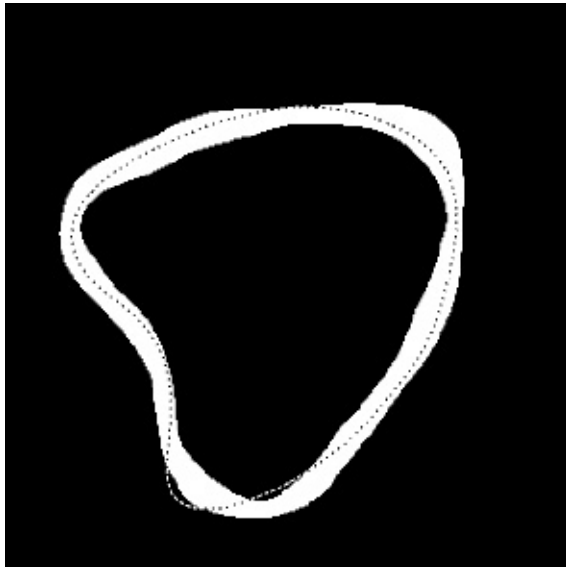


Figure 6. The 95% Bayesian credible interval for the boundary compared with the contour of the original object.

less than 0.025 lie outside the boundary of the object with very high probability (97.5%). The pixels with value greater than 0.975 almost certainly lie inside the boundary. The pixels that have a value between 0.025 and 0.975, shown in Fig. 6, comprise the central 95% credible interval¹⁵ for the boundary itself. In fact the portion of the original boundary that lies inside the 95% credible region is about 92% of the perimeter, in reasonably good agreement with the chosen credible interval. Note the varying width of the credible region in Fig. 6, which is related to the varying rms uncertainty noted above.

5. DISCUSSION

We have demonstrated the usefulness of deformable models in solving limit-angle tomographic reconstruction problems by using MCMC to assess the uncertainties associated with a reconstruction of a simple object from two views. Although an abundance of issues remain to be addressed, these results indicate the enormous promise of applying MCMC to Bayesian inference in medical imaging. This technique can obviously be used to estimate uncertainties in reconstructed (estimated) models. Moreover, it can be used to estimate the uncertainties in quantities derived from reconstructed models, e.g., ejection fraction of the heart, or the activity in a specified region of a reconstructed emission image.

A fundamental issue that we have not addressed in much detail is the selection of the hyperparameter α . We have chosen α on the basis of the degree of variation observed in the MCMC samples of the posterior, which indicates that the prior is not restricting the smoothness of the boundary very much. Since the value of α affects the width of the prior probability distribution, it influences the posterior uncertainty. Therefore, it is imperative to place more emphasis on understanding how to choose hyperparameters.⁶ We note that this problem is not confined to Bayesian analysis. As we argued in Sect. 3, choosing α is equivalent to selecting the number of degrees of freedom in the representation of the boundary description. Any successful treatment of ill-posed problems must employ a constraining model and hence must cope with the challenge of selecting the number of degrees of freedom.

In the present study α is fixed. A more appropriate approach would be to consider α as a parameter that should be determined from the data, which goes by the name of empirical Bayesian analysis. By including α in the list of variables to be sampled in the MCMC process, the uncertainty in α would be taken into account in the overall uncertainty analysis.

In the simulated example presented here, the background surrounding the object is truly zero. In medical imaging, one rarely encounters such an idealized situation. However, the flexibility of the Bayesian approach,

which we have attempted to incorporate into the BIE, allows one to augment a model to include other features, e.g., density outside the object used here. One should always check that the models used in an analysis properly match the data and take corrective actions if they don't.

The present analysis has assumed that the interior density of the object is known. This knowledge would not be available in most experimental situations. A more meaningful study would require the interior density to be estimated from the data, as well as the shape of the object. The expected increase in uncertainty in the boundary location would presumably be shown by an MCMC analysis that included variations in density in the trial steps.

Any estimates drawn from a finite MCMC sequence is subject to the uncertainty caused by the finite number of samples obtained from the posterior. One of the important issues concerning MCMC is how to estimate the accuracy of an uncertainty estimation, from the point of view of both statistical sampling and full coverage of the posterior bubble. Our simple example leads us to believe the efficiency of MCMC can be very poor, particularly when the Metropolis algorithm is used with steps drawn from an isotropic trial distribution. Minimizing the CPU time required to achieve a specified accuracy is of critical importance. One approach that seems promising is to make use of the gradient of the minus-log-posterior, a capability built into the BIE, to select the MCMC trial steps for improved efficiency.

In regard to the use of a polygon to represent a smooth curve, one would ideally like to reduce the length of the polygon sides to a size where this discretization does not affect the results. However, in the present formalism, shorter sides can lead to an increasing frustration of the MCMC algorithm, for example, because of the prior on side length described in Sect. 2.1. The result is that one is forced to use increasingly smaller MCMC steps, which leads to a reduced efficiency of the algorithm. One approach to overcoming this problem is to limit the direction of trial steps of each vertex to be along the bisector of angle between neighboring sides, somewhat like the suggestion of Lobregt and Viergever.²³ Another approach avoids the use of the prior on polygon side length by using adaptable discretization, either on an edge-by-edge basis²³ or by routinely resampling the full polygon boundary to create equal-length sides. Another means that warrants investigation is to use a multiresolution representation of the boundary. The advantage would be that one could adjust the size of the MCMC steps at each resolution to improve the overall efficiency of the posterior sampling algorithm.

Before concluding, we mention an alternative method of probing the posterior to estimate the uncertainty in specific aspects of an estimated model, which we introduced several years ago.^{24,11} In that approach, which we often refer to as the “hard truth” concept, one observes the displacement of the most probable model as one applies a specified “force” to the model. We have shown that the resulting displacement in the model parameters is quantitatively related to the covariance matrix times the force vector when the posterior can be approximated by a multivariate Gaussian distribution.

Acknowledgments

John Skilling alerted us to the inconsistency in the way we define the prior on curvature, but throw MCMC samples in terms of the vertex positions. Many other people have helped us understand MCMC and its potential usefulness, including Julian Besag, James Gubernatis, Richard Silver, and Roger Bilisoly.

REFERENCES

1. K. M. Hanson, “Reconstruction based on flexible prior models,” in *Image Processing*, M. H. Loew, ed., *Proc. SPIE* **1652**, pp. 183–191, 1992.
2. K. M. Hanson, “Bayesian reconstruction based on flexible prior models,” *J. Opt. Soc. Amer. A* **10**, pp. 997–1004, 1993.
3. M. Kass, A. Witkin, and D. Terzopoulos, “Snakes: active contour models,” *Inter. J. Comp. Vision* **1**, pp. 321–331, 1988.
4. R. Szeliski and D. Terzopoulos, “Physically-based and probabilistic models for computer vision,” *Proc. SPIE* **1570**, pp. 140–152, 1991.
5. K. M. Hanson, G. S. Cunningham, G. R. Jennings, Jr., and D. R. Wolf, “Tomographic reconstruction based on flexible geometric models,” in *Proc. IEEE Int. Conf. Image Processing, vol. II*, pp. 145–147, IEEE, 1994.

6. D. J. C. MacKay, "Bayesian interpolation," *Neural Computation* **4**, pp. 415–447, 1992.
7. D. S. Sivia, *Data Analysis: A Bayesian Tutorial*, Clarendon, Oxford Univ. Press, New York, 1996.
8. A. Gelman, J. B. Carlin, H. S. Stern, and D. B. Rubin, *Bayesian Data Analysis*, Chapman & Hall, London, 1995.
9. K. M. Hanson, G. S. Cunningham, and R. J. McKee, "Uncertainties in tomographic reconstructions based on deformable models," in *Image Processing*, K. M. Hanson, ed., *Proc. SPIE* **3034**, pp. 276–286, 1997.
10. K. M. Hanson, R. L. Bilisoly, and G. S. Cunningham, "Kinky tomographic reconstruction," in *Image Processing*, M. H. Loew and K. M. Hanson, eds., *Proc. SPIE* **2710**, pp. 156–166, 1996.
11. K. M. Hanson and G. S. Cunningham, "Exploring the reliability of Bayesian reconstructions," in *Image Processing*, M. H. Loew, ed., *Proc. SPIE* **2434**, pp. 416–423, 1995.
12. K. M. Hanson and G. S. Cunningham, "The Bayes Inference Engine," in *Maximum Entropy and Bayesian Methods*, K. M. Hanson and R. N. Silver, eds., pp. 125–134, Kluwer Academic, Dordrecht, 1996.
13. G. S. Cunningham, K. M. Hanson, G. R. Jennings, Jr., and D. R. Wolf, "An object-oriented implementation of a graphical-programming system," in *Image Processing*, M. H. Loew, ed., *Proc. SPIE* **2167**, pp. 914–923, 1994.
14. K. M. Hanson and G. S. Cunningham, "A computational approach to Bayesian inference," in *Computing Science and Statistics* **27**, M. M. Meyer and J. L. Rosenberger, eds., pp. 202–211, Interface Foundation, Fairfax Station, VA 22039-7460, 1996.
15. J. Besag, P. Green, D. Higdon, and K. Mengersen, "Bayesian computation and stochastic systems," *Stat. Sci.* **10**, pp. 3–66, 1995.
16. W. R. Gilks, S. Richardson, and D. J. Spiegelhalter, *Markov Chain Monte Carlo in Practice*, Chapman and Hall, London, 1996.
17. N. Metropolis, A. W. Rosenbluth, M. N. Rosenbluth, A. H. Teller, and E. Teller, "Equations of state calculations by fast computing machine," *J. Chem. Phys.* **21**, pp. 1087–1091, 1953.
18. K. M. Hanson and G. W. Wecksung, "Bayesian approach to limited-angle reconstruction in computed tomography," *J. Opt. Soc. Amer.* **73**, pp. 1501–1509, 1983.
19. K. M. Hanson, "Bayesian and related methods in image reconstruction from incomplete data," in *Image Recovery: Theory and Application*, H. Stark, ed., pp. 79–125, Academic, Orlando, 1987.
20. G. S. Cunningham and K. M. Hanson, "Uncertainty estimation for Bayesian reconstructions from low-count SPECT data," in *Conf. Rec. IEEE Nucl. Sci. Symp. and Med. Imaging Conf.*, IEEE, Piscataway, 1996.
21. K. M. Hanson and D. R. Wolf, "Estimators for the Cauchy distribution," in *Maximum Entropy and Bayesian Methods*, G. Heidbreder, ed., pp. 255–263, Kluwer Academic, Dordrecht, 1993.
22. K. J. Myers, R. F. Wagner, and K. M. Hanson, "Rayleigh task performance in tomographic reconstructions: comparison of human and machine performance," in *Image Processing*, M. H. Loew, ed., *Proc. SPIE* **1898**, pp. 628–637, 1993.
23. S. Lobregt and M. A. Viergever, "A discrete dynamic contour model," *IEEE Trans. Med. Imaging* **MI-14**, pp. 12–24, 1995.
24. K. M. Hanson and G. S. Cunningham, "The hard truth," in *Maximum Entropy and Bayesian Methods*, J. Skilling and S. Sibisi, eds., pp. 157–164, Kluwer Academic, Dordrecht, 1996.